Utilizing the solution of sound diffraction by a thin screen to evaluate infrasound waves attenuated around volcano topography

Kyoka Ishii[a,b,*], Akihiko Yokoo[a], Masato Iguchi[c], Eisuke Fujita[d]

[a] *Aso Volcanological Laboratory, Institute for Geothermal Sciences, Graduate School of Science, Kyoto University, 3028 Sakanashi, Ichinomiya-machi, Aso, Kumamoto, Japan*
[b] *Division of Earth and Planetary Sciences, Graduate School of Science, Kyoto University, Kitashirakawa Oiwake-cho, Sakyo-ku, Kyoto, Japan*
[c] *Sakurajima Volcano Research Center, Disaster Prevention Research Institute, Kyoto University, 1722-19 Sakurajima-Yokoyama, Kagoshima, Japan*
[d] *National Research Institute for Earth Science and Disaster Resillience, 3-1 Tennodai, Tsukuba, Ibaraki, Japan*

Abstract

The observation of infrasound signals in the vicinity of volcanoes is a powerful tool to understand the source of explosive volcanic activity. Although the propagation of infrasound signals is affected by the local topography, such effects are often ignored in the analysis, leading to potential misinterpretation of the source parameters. In this study, we propose a simple low-cost method of evaluating the attenuation of infrasound signals by topographical barriers. In this method, the first step approximates the elevation profile between the source and station into one thin screen-like barrier. Then, a mathematically exact solution of a sound diffraction problem is adopted to evaluate the attenuation of the infrasound amplitudes. To assess the validity of this method, the obtained estimates are compared with actual infrasound data observed at

*Corresponding author; ishii.kyoka.46m@st.kyoto-u.ac.jp

Sakurajima volcano, Japan. The results show that the estimates of relative amplitude to a reference station are more accurate than those considering only geometrical spreading, suggesting that the proposed method provides a useful first-order investigation of the attenuation of infrasound signals. The spatial distribution of the attenuation in the entire area of the volcano was also estimated, revealing a significant contrast between the eastern and western sides of the study area. Variations in signal attenuation also depend on the radial distance from the crater and were mainly attributed to variations of the relative screen height to the incident wavelength.

Keywords:
Infrasound, Diffraction, Signal attenuation, Volcano topography

---

Highlights

- Volcanic infrasound signals are attenuated by topographical barriers.
- Infrasound wave attenuation is estimated using a sound-diffraction-based method.
- Diffraction by topography is essential to estimate infrasound amplitudes.

1. Introduction

Infrasound signals (sound waves with frequencies < 20 Hz) generated by volcanic explosions contain information that directly reflect the explosive source processes at the crater. Observed amplitudes of infrasound records can be converted into a number of physical quantities, such as the volumetric flow rate of gas emissions into the atmosphere (Johnson, 2003; Johnson et al., 2004) and the volume of gas slugs breaking into discrete explosions (Delle Donne et al., 2016). These conversions can further our understanding of the source processes of volcanic eruptions. Therefore, during the last decade, observations of infrasound pressure fluctuations have become an important tool for the interpretation of various eruptive phenomena and have been conducted at volcanoes worldwide (Garcés et al., 2013; Matoza et al., 2019).

Aiming to derive source parameters from observed infrasound records, the effects on their propagation from the source to a station need to be considered. It is generally assumed that an infrasound wave radiates from a monopole source that is either an isotropic gas expansion in a Strombolian explosion or a transient gas emission with an acceleration of the volumetric flow rate (e.g., Vergniolle and Brandeis, 1994; Johnson et al., 2008; Johnson and Miller, 2014). On this assumption, the observed amplitude of the infrasound wave is proportional to the inverse of the distance between a source and station based on geometrical spreading (Lighthill, 1978). Many studies have adopted this relationship to estimate the volumetric flow rate from infrasound data (Johnson, 2003; Johnson et al., 2004; Johnson and Miller, 2014). To simplify data processing, effects other than geometrical spreading tend to be ignored. It is known, however, that infrasound signals are affected by the atmospheric structure and local topography (Fee and Matoza, 2013; Matoza et al., 2019). Vertical profiles of air temperature and wind speed can provide wave refraction (Fee and Garcés, 2007; Lacanna et al., 2014). In addition, infrasound waves are often diffracted and reflected due to topographical barriers of volcanoes such as crater rims, ridges, and hills (Kim and Lees, 2011;

Kim et al., 2012; Lacanna and Ripepe, 2013). In recent years, these effects have been incorporated into numerical simulations of wave propagation reflecting the development of finite-difference time-domain (FDTD) simulation techniques (Kim and Lees, 2011, 2014; Matoza et al., 2009). While the impact of the atmospheric structure is evident for long-distance propagation of infrasound waves (de Groot-Hedlin et al., 2011; Lacanna et al., 2014), the atmospheric contribution is often ignored in cases of local infrasound observations because it has negligible effects on the signals (Kim et al., 2015; Fee et al., 2017; Iezzi et al., 2019). On the other hand, ignoring the effects of topography near the source can be problematic, leading to over- or underestimation of the volumetric flow rate (Kim et al., 2015). Therefore, for a more quantitative discussion of the source processes of volcanic explosions, the topographical effects should be included in the analysis of such infrasound data (Lacanna and Ripepe, 2013).

Three-dimensional (3-D) FDTD simulations of infrasound propagation are an effective way to evaluate the topographical effects on the observed data. However, the costs of such numerical simulations are high. Although a 2-D FDTD simulation is not too difficult to perform on a personal computer (Lacanna and Ripepe, 2013), the 3-D simulation needs substantial computational resources, including calculation space and time (Kim and Lees, 2014). To reduce calculation costs, additional graphics processing units were used for parallel calculations by Kim and Lees (2014). A simple way to quantitatively evaluate the effects of topography on the infrasound propagation, without any high-cost numerical simulations, would allow the estimation of source parameters effortlessly. For example, such a simple method could be helpful for a scenario of a rapidly changing crater geometry resulting from successive eruptions. In addition, it would provide an indicator of the topographical effect when searching for suitable positions of infrasound stations in advance.

In this study, a simple method for the evaluation of topographical impacts on infrasound signals is proposed. In general, a sound wave, which usually refers to audible bands with frequencies of 20 Hz – 20 kHz, propagating outdoors interacts with the topography in various ways (refer to review papers; e.g., Embleton, 1996). For example, 1) a topographical barrier attenuates the observed amplitudes, 2) some signals can be amplified by superposition of reflected waves at topographic irregularities, 3) a sound wave scatters on uneven ground, or 4) a sound field near the ground depends on the acoustic impedance of the ground. Here, the focus is primarily on the attenuation of amplitudes by topographical barriers between the infrasound source and the station as a first step. Lacanna and Ripepe (2013) reported that the observed amplitude of infrasound signals at a volcanic field is attenuated compared with the estimated values from geometrical spreading. However, the quantitative prediction of such attenuations has been difficult. Theoretically, sound diffraction by a simply shaped obstacle (e.g., a thin screen or a wedge) has been well studied by acousticians (e.g., Pierce, 1989). Moreover, the sound field affected by an obstacle with a complicated shape, such as a mountain or building, can be estimated by approximating its shape to a simple one (Maekawa, 1968). Based on this idea, the volcanic topographical barriers are simplified as one screen like a thin noise barrier. The attenuation of the amplitude of the infrasound signals is assessed by applying an exact solution of a diffraction problem (Macdonald, 1915). Then, the estimation results are compared with actual infrasound data acquired at Sakurajima volcano to confirm the validity of the proposed method. Specifically, we determine whether our method can provide better amplitude estimates than the method considering only geometrical spreading. In addition, we investigate the most effective topographic characteristics for attenuation of infrasound signals at volcanic fields.

2. Attenuation of infrasound amplitude based on the solution of the diffraction problem

A solution of the diffraction problem of a sound wave was applied to estimate the attenuation of infrasound signals by the topographical barriers of volcanoes. The most typical and fundamental problem of sound diffraction is wave diffraction by a semi-infinite thin screen (Fig. 1a). For the estimation of the signal attenuation, a classic and primary mathematical exact solution of this setting was adopted (Macdonald, 1915; Bowman and Senior, 1969). This solution is used to this day for assessments of approximate schemes or numerical simulations (e.g., Menounou, 2001; Li and Wong, 2005). It assures highly accurate estimations regardless of the positions of source and receiver relative to a screen (Kawai and Itow, 1976).

First, the pressure field p_0 in the vicinity of a harmonic monopole source was assumed to be given by

$$p_0 = \frac{\mathrm{e}^{\mathrm{i}kR}}{4\pi R}, \tag{1}$$

where R is the distance from the source to the receiver and k the wavelength. For simplicity, a time-dependent factor of $\mathrm{e}^{-\mathrm{i}\omega t}$ (ω is angular frequency) was omitted from the equation. In this case, Macdonald's rigorous solution provides a theoretical pressure field p affected by a rigid semi-infinite screen as follows (Li and Wong, 2005):

$$p = \frac{\mathrm{i}k}{4\pi}\int_{\varsigma_1}^{\infty}\frac{H_1^{(1)}(kR+s^2)}{\sqrt{s^2+2kR}}\mathrm{d}s + \frac{\mathrm{i}k}{4\pi}\int_{\varsigma_2}^{\infty}\frac{H_1^{(1)}(kR_\mathrm{m}+s^2)}{\sqrt{s^2+2kR_\mathrm{m}}}\mathrm{d}s, \tag{2}$$

$$\varsigma_1 = \mathrm{sgn}(|\theta_\mathrm{s}-\theta_\mathrm{r}|-\pi)\sqrt{k(R'-R)}, \tag{3}$$

$$\varsigma_2 = \mathrm{sgn}(\theta_\mathrm{s}+\theta_\mathrm{r}-\pi)\sqrt{k(R'-R_\mathrm{m})}, \tag{4}$$

where R_m is the image source–receiver distance and R' the shortest distance from the source to the receiver over the top of the screen (Fig. 1a). $H_1^{(1)}$ is the Hankel function of the first kind. In Eqs. (3) and (4), sgn is the sign function and θ_s and θ_r are the angles formed by the screen and the source, and the receiver, respectively, in a counterclockwise direction (Fig. 1a). Eq. (2) shows that the sound field is composed of two integrals; the first term corresponds to the contribution of the source, the second term accounts for that of the image source. These integrals are related to the integral representation of a spherical wave in the cylindrical polar system (Li and Wong, 2005). The pressure p_0 in Eq. (1) decays with increasing distance (geometrical spreading), while the pressure p in Eq. (2) is further impacted by a semi-infinite screen inserted between a source and receiver.

If a screen stands on the ground, the signal reflection at the ground should be considered. In this case, there are four sound rays from a source to a receiver (Fig. 1b) and they are interfering each other: (i) a direct ray, (ii) a ray reflected at the source side, (iii) a ray reflected at the receiver side, and (iv) a ray reflected at both sides. Generally, for infrasound observations at volcanoes, both the source and the observation station are assumed to be on the ground. In these situations, assuming that the ground is rigid, all four rays should theoretically become coherent (Kurze, 1974). As a result, the observed pressure with the screen on the ground p_{w} can be obtained by simply quadrupling the amplitude of the pressure p from Eq. (2):

$$\begin{aligned} p_{\mathrm{w}} &= 4p \\ &= \frac{\mathrm{i}k}{\pi}\int_{\varsigma_1}^{\infty}\frac{H_1^{(1)}(kR+s^2)}{\sqrt{s^2+2kR}}\mathrm{d}s + \frac{\mathrm{i}k}{\pi}\int_{\varsigma_2}^{\infty}\frac{H_1^{(1)}(kR_{\mathrm{m}}+s^2)}{\sqrt{s^2+2kR_{\mathrm{m}}}}\mathrm{d}s. \end{aligned} \tag{5}$$

However, a problem arises when the height of the screen is very low, probably due to the approximate nature of this approach. Assuming the pressure p_{wo} generated by a monopole source on the ground (i.e., a monopole source in a half-space without a screen) as

$$p_{\mathrm{wo}} = 2p_0, \tag{6}$$

the pressure p_{w} is expected to converge into p_{wo} by bringing R' close to R in Eq. (5) (i.e., the height of the screen is set to zero on the ground). However, the contribution of the second term of Eq. (5) does not vanish as anticipated and the convergence into p_{wo} does not happen, leading to an overestimation of the pressure amplitude. To resolve this problem, no screen was installed for relative heights of the screen to wavelength < 0.1.

In order to quantify the attenuation of the infrasound amplitude by a screen on the ground, an indicator α was defined as:

$$\alpha = \left|\frac{p_{\mathrm{w}}}{p_{\mathrm{wo}}}\right| = \left|\frac{4p}{2p_0}\right|. \tag{7}$$

Here, α is the ratio of the amplitude affected by both a topographical barrier and geometrical spreading to the amplitude only affected by geometrical spreading. The smaller α, the more the amplitude is attenuated by the topography. According to Eqs. (5) and (7), α depends on four variables: R, R_{m}, R', and k. To intuitively understand features of α, these variables were transformed into four different variables: the source-receiver distance on the ground L, the source-screen distance L', the screen height H, and the wavelength of the incident wave λ (Fig. 2a). To investigate how α depends on these alternative variables, they were normalized as L/λ, H/λ, and L'/L (Fig. 2b–e). In most cases, infrasound observation stations in the vicinity of volcanoes are located a few hundred meters to a few kilometers away from a source to target signals with main energy concentrations of < 5 Hz (e.g., Johnson and Ripepe, 2011). Therefore, when assuming that L is 0–5000 m and λ is 50–500 m, L/λ becomes 0–100. According to the reciprocal property of Green's function (Morse and Ingard, 1986), L'/L can be 0–0.5. The screen height H was changed to satisfy $H/L < 1$. When these parameters vary in the above ranges, α becomes small (i.e., the amplitude is more attenuated) as the relative height of the screen to the wavelength H/λ increases (Fig. 2b, c). With constant H/λ, α increases with the growth of L/λ, but the rate of increase gradually decreases (Fig. 2d). The variation of L'/L does not significantly affect the value of α in $L/\lambda < 10$ (Fig. 2c, e).

3. Validation of the proposed method

In order to evaluate the proposed method for estimating the attenuation of infrasound signals, the synthetic amplitudes at infrasound stations around Sakurajima volcano, Japan, were calculated and the results compared with the observed data. In a study of acoustics, Maekawa (1968) suggested that the reduction of signal amplitude can be estimated by approximating a topographical barrier to an equivalent screen. Following this idea, each topographical profile between the source and nine stations around Sakurajima (Fig. 3a) was simplified into a single thin screen (Fig. 3b). Eq. (5) was used for the estimation, assuming that a monopole source was situated at the active Showa crater located on the eastern flank of the volcano (Fig. 3a). The wavelength of the incident wave was 680 m (0.5 Hz at the speed of sound in air 340 m/s), which is comparable to the dominant frequency of actual infrasound data. The elevation profile between the source and each station was approximated by a screen perpendicular to the slanted line directly connecting the source and the station (Fig. 3b). The height of each screen was defined as the maximum relative height from the slanted line in the elevation profile. The screen was set at the position of maximum relative height. A high-resolution (5 m) digital elevation model (DEM) was used for the calculation. This DEM combined a 10-m DEM of the entire area of Sakurajima published by the Geospatial Information Authority of Japan in 2012 and a 5-m DEM around the crater acquired during laser surveys conducted by the Japanese Ministry of Land, Infrastructure, Transport and Tourism in October 2016.

Infrasound data of 31 Vulcanian explosions that occurred at the Showa crater from August 31 to September 26, 2017 were used for evaluation. The energy of infrasound signals was concentrated at frequencies < 0.8 Hz and mainly between 0.4 Hz and 0.5 Hz. In this study, we used amplitudes of 0.5 Hz in the frequency domain as a representative value because the dominant frequency observed at the majority of stations was 0.5 Hz. The example at a frequency of 0.4 Hz is shown in a supplementary file. This frequency component was transformed from the waveform of the 10-s window from 2 s before the arrival time of signals. To compare the estimated and observed amplitudes, the amplitudes at all stations were normalized using those at the KUR station ($|p_{\mathrm{w}}/p_{\mathrm{w}}^{\mathrm{KUR}}|$) for each event. The KUR station is commonly used as a reference station because it is located on the line-of-sight from the Showa crater (Yokoo et al., 2014; Johnson and Miller, 2014).

To assess whether the estimates match the observed relative amplitudes of the infrasound data, the standard deviation distance S was applied. The standard deviation distance is defined as $S = |X - \mu|/\sigma$ where X is the estimated amplitude, and μ and σ are the average and standard deviation of the observed amplitudes, respectively. This indicates whether a sample is included in a population assumed to have a normal distribution. Almost all samples (99.7%) in the population lie within a range of $S < 3$ (i.e., where the difference from the mean is within $\pm 3\sigma$).

A comparison of the obtained estimates with the observed data shows that the estimated relative amplitudes are closer to the observed data at most stations than those based on the geometrical spreading consideration alone (Fig. 3c, Table 1). The decaying amplitudes expected from geometrical spreading ($1/R$) are illustrated by a black line in Fig. 3c, and are not compatible with the observed values at the KIT, ARI, HAR, SET, and SVO stations. Especially at KIT and SVO, however, our estimates fall in the range of $\pm 3\sigma$ of the observed distributions. Although the estimates at ARI and HAR are out of the range of $\pm 3\sigma$ of the observation, the values of S are substantially improved compared to those of $1/R$. However, the S at SET does not change considerably between the estimate using the screen and $1/R$, and is also out of the range of $\pm 3\sigma$. The values of α at the stations on the western side of Sakurajima volcano (HAR, SVO) are $\sim$0.6, in contrast to 0.8–1 at the stations on the eastern side (Table 1). In particular, the difference in α between HAR (on the western side) and KUR (on the eastern side) is significant ($\sim$0.4), even though the difference in the slanted distance from the source to the stations is only a few percent (Fig. 3b).

These results suggest that the proposed method is useful as a first step for estimating infrasound relative amplitudes observed around volcanoes. In the estimation, only sound diffraction by a simple screen is considered, whereas fine-scale undulations of topographic relief or 3-D propagation effects such as wrap-around waves and reflection of infrasound signals are ignored. Nevertheless, the calculated relative amplitudes are better than those derived by considering geometrical spreading alone at almost all stations around Sakurajima volcano. Moreover, our estimates are within the range of $\pm 3\sigma$ of the observation at five out of eight stations. Therefore, an infrasound relative amplitude observed at a station can be estimated as a first-order approximation by considering attenuation by topographical barriers in addition to geometrical spreading. In other words, the two factors of geometrical spreading and attenuation by topography should be considered as a priority when estimating the approximate spatial distribution of infrasound signals.

However, it is important to note that the estimated amplitudes at ARI, HAR, and SET stations do not fall in the observed ranges. These discrepancies between the estimates and observations cannot be explained by a change of the effective sound speed (supplementary file). Therefore, we conclude that such discrepancies may be caused by ignoring the 3-D topography. The relative amplitudes estimated from 3-D numerical simulations of infrasound propagation are within the range of the observed distribution at all stations (supplementary file). Further investigation into the type of topography that leads to such discrepancies would improve our understanding of the topographic impact on infrasound propagation.

4. Control parameter of the spatial change of infrasound signal attenuation

To better understand how the attenuation of infrasound signals changes spatially in a real volcanic environment, the spatial distribution of α was calculated for the entire area of Sakurajima volcano. To this end, the pressure amplitudes (p_{wo} and p_{w} from Eqs. (5) and (6)) were estimated at each node in a grid with 200 m spacing. These pressures are generated from a monopole source (infrasound wave with $\lambda = 680$ m) situated inside the Showa crater. When only geometrical spreading is considered, as is usually the case in volcanic infrasound studies (e.g., Johnson, 2003), the distribution of p_{wo} shows a concentric pattern centered in the crater (Fig. 4a). On the other hand, the distribution pattern of the pressure p_{w} resulting from the insertion of the screen is highly distorted on the western side of the crater (Fig. 4b). The ratio of these two pressures denoted by α (Eq. (7)) ranges from 0.49 – 1 in the entire area. A notable feature in the spatial distribution map of α is a significant contrast ($\sim$0.4) between the eastern and western side of Sakurajima (Fig. 4c). Its boundary appears to cross the summit of the volcano roughly in a north-south direction.

Fig. 4c also shows how α changes with the radial distance from the source in all four geographic directions (north, south, east, and west). The value of α drastically drops (20–50%) with increasing distance from the source, however, its variation becomes limited with increasing distance. For example, in the westward direction (top panel of Fig. 4c), α decreases at a pace of $\sim$0.3/km until 2 km is reached. At distances $>$ 2 km, α slightly increases ($\sim$0.02/km) at a pace one order of magnitude smaller than that near the source. The changing rates of α between the near and far ranges in the other three geographic directions also differ by one order of magnitude.

Variations of α with the radial distance are similar in all directions (Fig. 5a, b). As mentioned in section 2, the value of α can be described by three normalized parameters, L/λ, H/λ, and L'/L (Fig. 2). Using L/λ instead of the exact horizontal distance, a sharp drop and subsequent slight increase of α at small and large L/λ are recognized, corresponding to variations seen in Fig. 4c (Fig. 5a, b). Although the exact position of α's turning point is not constant for all directions, it seems to correspond to the maximum of H/λ in each radial variation (circles in Fig. 5c, d). Hereafter, this point is referred to as point Q. While the point Q's in the radial changes of α on the western side of Sakurajima volcano (red lines in Fig. 5a, b) are highly scattered in the range of $L/\lambda \geq 3$, those on the eastern side (blue lines) are concentrated where L/λ ranges between 1 and 3.

The observed radial variations of α can be explained by the radial variation of H/λ. In the case of the Sakurajima volcano, the three normalized parameters, L/λ, H/λ, and L'/L, range between 0–10, 0–1, and 0–0.5, respectively. Within these ranges, the change of L'/L hardly affects α (Fig. 2c, e). Therefore, the radial variation of α mainly depends on the variation of H/λ with increasing L/λ. Where L/λ is smaller than L/λ at point Q (close to the crater), H/λ rapidly increases (Fig. 5c). This change of H/λ causes the observed distinct decrease of α (Fig. 2b). On the other hand, beyond point Q, H/λ is almost constant with increasing L/λ (Fig. 5d), resulting in a low changing rate for α at greater distances (Fig. 2d).

Moreover, the radial variations of H/λ depend on the geographic direction from the crater. In particular, the variations to the west of the volcano conspicuously differ from those to the east (Fig. 5c, d). This is probably due to the crater being located on the eastern flank of the volcano (Fig. 3a). On the western side of the crater, a high-elevation summit area causes increasing values of the relative height of screen H/λ for a few km (until $L/\lambda > 3$) (Fig. 5c). On the opposite side, however, no unique obstacles, with the exception of the crater rim, exist. Consequently, the increase of H/λ suddenly stops near the crater (where L/λ ranges between 1 and 3) (Fig. 5d). This difference in the spatial elevation profile between the eastern and western sides of the volcano yields the apparent directivity of the attenuation of infrasound waves (Fig. 4c). It also suggests that H/λ is the more effective parameter for the attenuation of infrasound signals at volcanic sites.

5. Conclusion

The attenuation of the amplitude of infrasound signals caused by topographical barriers at a volcano was evaluated by applying a simple method based on the exact solution of a fundamental sound diffraction problem. In this method, the topographical profile between a source and a station was simplified as a single thin screen. Validation of the proposed method using infrasound data from stations around Sakurajima volcano revealed that the estimated relative amplitudes were closer to the observed distributions than those estimated by considering geometrical spreading alone. Therefore, the proposed method is useful as a first step for estimating the spatial distribution of infrasound signals without the need for costly numerical simulations. In other words, geometrical spreading and attenuation by topographical barriers are thought to be the first and second most important factors controlling the approximate spatial distribution of infrasound signals. Moreover, the spatial distribution of the attenuation indicator α at Sakurajima volcano, i.e., the ratio of the amplitudes with and without the screen, showed a significant contrast between the eastern and western sides of the volcano. In the radial direction from the crater, the changing rate of α between near and far ranges is different by one order of magnitude. These characteristics of α's variation mainly result from the change of the normalized parameter H/λ, the relative height of the screen to the wavelength of the infrasound signal.

The proposed method can provide the spatial distribution of infrasound signals without the need for costly simulation. This distribution would help to search for proper areas for infrasound observation or to interpret the amplitude difference between different stations. However, the applicability of the proposed method to other volcanoes has not yet been confirmed. Future research should confirm the validity of the proposed method by investigating whether the estimation results match actual infrasound data at other volcano sites with more complex topographies. If the actual data have a different dominant frequency from the one discussed in this study (0.5 Hz), such data will be more suitable to identify the limitations of this method. For comparison between observations and estimates, relative amplitudes to the reference station were used in this study. Thus, even if over- or underestimates occur at all stations, these estimation errors could be canceled by scaling the estimated amplitudes to a reference value. Therefore, further evaluation of the absolute amplitudes would be necessary to further develop this method.

Acknowledgements

We thank T. Yamada for helping share the data and calibrate the sensors. We received generous support from T. Ohkura and the staff of Aso Volcanological Laboratory. We also thank the anonymous reviewers for their insightful comments. This work was financially supported by the Ministry of Education, Culture, Sports, Science and Technology of Japan under its Earthquake and Volcano Hazards Observation and Research Program, and JSPS grant 19K03992. The 5-m DEM used in this study was provided by the Japanese Ministry of Land, Infrastructure, Transport and Tourism.

Reference

Bowman, J.J., Senior, T.B., 1969. Electromagnetic and Acoustic Scattering by Simple Shapes. North-Holland, Amsterdam.

Delle Donne, D., Ripepe, M., Lacanna, G., Tamburello, G., Bitetto, M., Aiuppa, A., 2016. Gas mass derived by infrasound and UV cameras: Implications for mass flow rate. Journal of Volcanology and Geothermal Research 325, 169–178. doi:10.1016/j.jvolgeores.2016.06.015.

Embleton, T.F., 1996. Tutorial on sound propagation outdoors. The Journal of the Acoustical Society of America 100, 31–48. doi:10.1121/1.415879.

Fee, D., Garcés, M., 2007. Infrasonic tremor in the diffraction zone. Geophysical Research Letters 34, L16826. doi:10.1029/2007GL030616.

Fee, D., Izbekov, P., Kim, K., Yokoo, A., Lopez, T., Prata, F., Kazahaya, R., Nakamichi, H., Iguchi, M., 2017. Eruption mass estimation using infrasound waveform inversion and ash and gas measurements: Evaluation at Sakurajima volcano, Japan. Earth and Planetary Science Letters 480, 42–52. doi:10.1016/j.epsl.2017.09.043.

Fee, D., Matoza, R.S., 2013. An overview of volcano infrasound: from hawaiian to plinian, local to global. Journal of Volcanology and Geothermal Research 249, 123–139. doi:10.1016/j.jvolgeores.2012.09.002.

Garcés, M.A., Fee, D., Matoza, R., 2013. Volcano acoustics, in: Fagents, S., Gregg, T., Lopes, R. (Eds.), Modeling Volcanic Processes: The Physics and Mathematics of Volcanism. Cambridge University Press, pp. 359–383.

de Groot-Hedlin, C., Hedlin, M.A., Walker, K., 2011. Finite difference synthesis of infrasound propagation through a windy, viscous atmosphere: application to a bolide explosion detected by seismic networks. Geophysical Journal International 185, 305–320. doi:10.1111/j.1365-246X.2010.04925.x.

Iezzi, A., Fee, D., Kim, K., Jolly, A., Matoza, R., 2019. 3-D acoustic multipole waveform inversion at Yasur volcano, Vanuatu. Journal of Geophysical Research: Solid Earth 124, 8679–8703. doi:10.1029/2018JB017073.

Johnson, J., Aster, R., Jones, K.R., Kyle, P., McIntosh, B., 2008. Acoustic source characterization of impulsive Strombolian eruptions from the Mount Erebus lava lake. Journal of Volcanology and Geothermal Research 177, 673–686. doi:10.1016/j.jvolgeores.2008.06.028.

Johnson, J.B., 2003. Generation and propagation of infrasonic airwaves from volcanic explosions. Journal of Volcanology and Geothermal Research 121, 1–14. doi:10.1016/S0377-0273(02)00408-0.

Johnson, J.B., Aster, R.C., Kyle, P.R., 2004. Volcanic eruptions observed with infrasound. Geophysical Research Letters 31, L14604. doi:10.1029/2004GL020020.

Johnson, J.B., Miller, A.J., 2014. Application of the monopole source to quantify explosive flux during Vulcanian explosions at Sakurajima volcano (Japan). Seismological Research Letters 85, 1163–1176. doi:10.1785/0220140058.

Johnson, J.B., Ripepe, M., 2011. Volcano infrasound: a review. Journal of Volcanology and Geothermal Research 206, 61–69. doi:10.1016/j.jvolgeores.2011.06.006.

Kawai, T., Itow, T., 1976. Sound diffraction by a thin half-plane. The Journal of the Acoustical Society of Japan 32, 319–327. doi:10.20697/jasj.32.5_319.

Kim, K., Fee, D., Yokoo, A., Lees, J.M., 2015. Acoustic source inversion to estimate volume flux from volcanic explosions. Geophysical Research Letters 42, 5243–5249. doi:10.1002/2015GL064466.

Kim, K., Lees, J.M., 2011. Finite-difference time-domain modeling of transient infrasonic wavefields excited by volcanic explosions. Geophysical Research Letters 38, L06804. doi:10.1029/2010GL046615.

Kim, K., Lees, J.M., 2014. Local volcano infrasound and source localization investigated by 3D simulation. Seismological Research Letters 85, 1177–1186. doi:10.1785/0220140029.

Kim, K., Lees, J.M., Ruiz, M., 2012. Acoustic multipole source model for volcanic explosions and inversion for source parameters. Geophysical Journal International 191, 1192–1204. doi:10.1111/j.1365-246X.2012.05696.x.

Kurze, U.J., 1974. Noise reduction by barriers. The Journal of the Acoustical Society of America 55, 504–518. doi:10.1121/1.1914528.

Lacanna, G., Ichihara, M., Iwakuni, M., Takeo, M., Iguchi, M., Ripepe, M., 2014. Influence of atmospheric structure and topography on infrasonic wave propagation. Journal of Geophysical Research: Solid Earth 119, 2988–3005. doi:10.1002/2013JB010827.

Lacanna, G., Ripepe, M., 2013. Influence of near-source volcano topography on the acoustic wavefield and implication for source modeling. Journal of Volcanology and Geothermal Research 250, 9–18. doi:10.1016/j.jvolgeores.2012.10.005.

Li, K., Wong, H., 2005. A review of commonly used analytical and empirical formulae for predicting sound diffracted by a thin screen. Applied Acoustics 66, 45–76. doi:10.1016/j.apacoust.2004.06.004.

Lighthill, M.J., 1978. Waves in Fluids. Cambridge University Press, New York.

Macdonald, H., 1915. A class of diffraction problems. Proceedings of the London Mathematical Society 2, 410–427. doi:10.1112/plms/s2_14.1.410.

Maekawa, Z., 1968. Noise reduction by screens. Applied Acoustics 1, 157–173. doi:10.1016/0003-682X(68)90020-0.

Matoza, R., Fee, D., Green, D., Mialle, P., 2019. Volcano infrasound and the international monitoring system, in: Le Pichon, A., Blanc, E., Hauchecorne, A. (Eds.), Infrasound Monitoring for Atmospheric Studies. Springer, pp. 1023–1077. doi:10.1007/978-3-319-75140-5_331023.

Matoza, R.S., Garcés, M.A., Chouet, B.A., D'Auria, L., Hedlin, M.A., Groot - Hedlin, C.D., Waite, G.P., 2009. The source of infrasound associated with long-period events at Mount St. Helens. Journal of Geophysical Research: Solid Earth 114, B04305. doi:10.1029/2008JB006128.

Menounou, P., 2001. A correction to Maekawa's curve for the insertion loss behind barriers. The Journal of the Acoustical Society of America 110, 1828–1838. doi:10.1121/1.1398050.

Morse, P.M., Ingard, K.U., 1986. Theoretical Acoustics. Princeton university press, Princeton.

Pierce, A.D., 1989. Acoustics: An Introduction to its Physical Principles and Applications. Acoustical Society of America, New York.

Vergniolle, S., Brandeis, G., 1994. Origin of the sound generated by Strombolian explosions. Geophysical Research Letters 21, 1959–1962. doi:10.1029/94GL01286.

Yokoo, A., Suzuki, Y.J., Iguchi, M., 2014. Dual infrasound sources from a Vulcanian eruption of Sakurajima volcano inferred from cross-array observation. Seismological Research Letters 85, 1212–1222. doi:10.1785/0220140047.

Figure captions

Fig. 1 Schematic models for the diffraction of the sound wave by a screen. (a) A semi-infinite screen is installed between a source and receiver. The source and the image source are linearly symmetrical with the screen. R, R_{m}, and R' are the source-receiver distance, the image source-receiver distance, and the shortest distance from the source to the receiver over the top of the screen, respectively. θ_{s} is the angle from the screen to the source in a counterclockwise direction, and θ_{r} is the angle formed between the screen and the receiver. (b) When a screen stands on the ground, there are four sound rays from the source to the receiver. One is (i) the direct ray from the source to the receiver (red line), while (ii)-(iv) the others are reflected on the ground at the source side (red dashed line), at the receiver side (black dashed line), and at both sides (black line), respectively. When both the source and the receiver are close to the ground, these four rays become coherent.

Fig. 2 The attenuation indicator α depends on three normalized parameters, L/λ, H/λ, and L'/L.
(a) The screen standing on the ground is characterized by three parameters: the distance from a source to a receiver L, that from a source to a screen L', and the height of a screen H. λ is the incident wavelength. (b), (c) The variations of the value of α depend on those parameters. They range between 0–100 (L/λ), 0–15 (H/λ), and 0–0.5 (L'/L), assuming the deployment of infrasound stations in the vicinity of volcanoes. H and L satisfy $H/L < 1$. α decreases with increasing H/λ under fixed values of L'/L (0.01, 0.1, and 0.5) and L/λ (1, 10, and 100). (d), (e) The variations of α at $L/\lambda < 10$. While α increases with L/λ, its increasing rate gradually decreases. The variation of L'/L does not have a large impact on α in this range as shown in (e).

Fig. 3 Infrasound observation in Sakurajima volcano.
(a) Map of nine infrasound stations at Sakurajima volcano. White squares indicate temporary stations installed from August 31 to September 26, 2017. Black and gray squares are permanent stations installed by the Disaster Prevention Research Institute of Kyoto University and the National Research Institute for Earth Science and Disaster Resilience, respectively. The Showa crater is located on the eastern flank of the volcano, where Vulcanian explo-

sions frequently occurred during our observation period in 2017. (b) The relative height of topographical profiles between the source and stations (HAR, KUR, and JIG). These profiles are rotated around the source so that the source and a station are on the same horizontal line. The screens (vertical black line) were installed at the positions where the relative height of the topography reaches the maximum value in each profile. Its height equals the screen's height. (c) Comparison between the estimated and observed amplitudes of infrasound signals. The amplitudes are normalized to the value at KUR station located on the line-of-sight from the Showa crater. Histograms show the distributions of observed amplitudes of 31 explosion events. Red circles indicate the estimated pressure amplitudes with screens ($|p_{\mathrm{w}}/p_{\mathrm{w}}{}^{\mathrm{KUR}}|$). The decaying amplitude considering only geometrical spreading is also shown as a solid line. The estimated values are closer to the observations than those derived by considering geometrical spreading alone at most stations.

Fig. 4 Estimated amplitudes in the entire area of Sakurajima volcano. (a) The distribution of pressure without the screen p_{wo} estimated from Eq. (6). The infrasound source is located in the Showa crater (the intersection of dashed lines). The pressure is calculated at each grid node with 200 m spacing. Its distribution represents a concentric pattern centered in the crater because the pressure decays inversely with the distance from the source to the node. (b) The distribution of pressure with the screen p_{w} (Eq. (5)). Compared to (a), the distribution is highly distorted on the western side of the crater. (c) The 2-D spatial and horizontal distributions of α ($= |p_{\mathrm{w}}/p_{\mathrm{wo}}|$; Eq. (7)) in Sakurajima. In the top view, the darker color indicates that observed amplitudes are well attenuated. There is a significant contrast of

α between the eastern and western sides of the crater. In the horizontal distributions in the top and side panels, α characteristically changes with distance from the crater for all four geographic directions (north, south, east, and west). Although α significantly decreases near the source (0.1–0.4/km), it increases slightly far from the source (0.005–0.04/km).

Fig. 5 Radial variations of α and H/λ against L/λ.
(a), (b) Radial distributions of α. Red lines represent the variations west of the crater, blue lines east of it. The changing trends of α are divided into two parts before and beyond the point Q's (circles), where H/λ reaches the maximum in each direction (c, d). In the area closer to the crater than point Q (a), α drops considerably with increasing L/λ. Beyond point Q, α slightly increases (b). The value of α on the western side of the volcano is $\sim$0.4 smaller than that on the eastern side. (c), (d) Radial distributions of H/λ before and beyond the point Q's. H/λ increases near the source, but becomes almost constant at a distance.

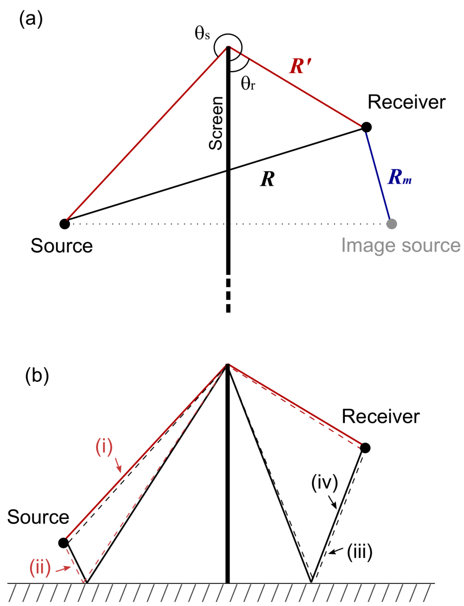

Figure 1: Schematic models for the diffraction of the sound wave by a screen.

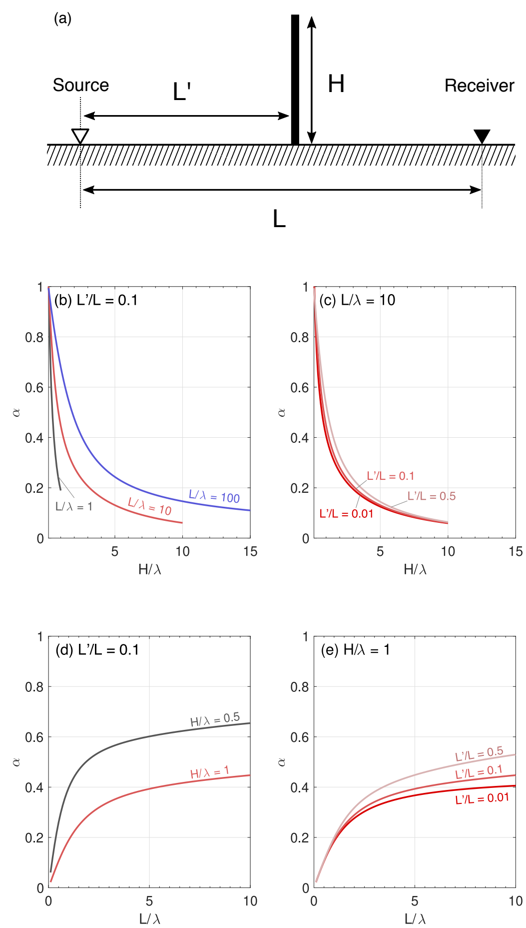

Figure 2: The attenuation indicator α depends on three normalized parameters, L/λ, H/λ, and L'/L.

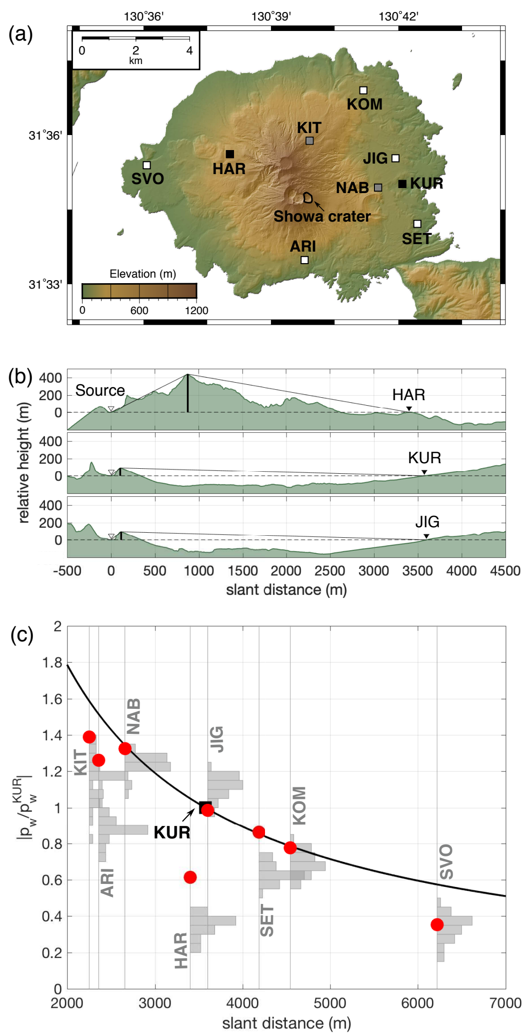

Figure 3: Infrasound observation in Sakurajima volcano.

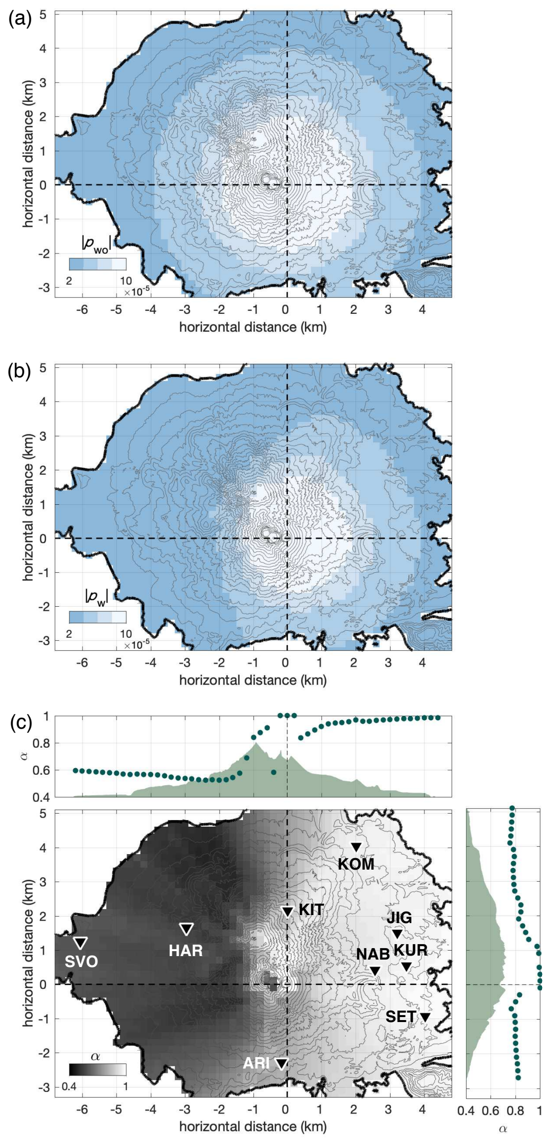

Figure 4: Estimated amplitudes in the entire area of Sakurajima volcano.

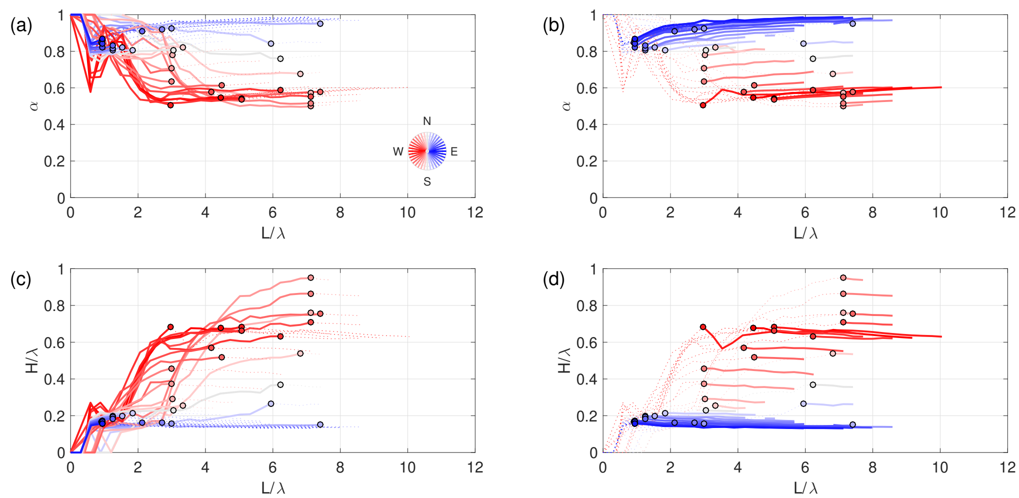

Figure 5: Radial variations of α and H/λ against L/λ.

Table 1: Standard deviation distances S at infrasound stations around Sakurajima volcano.

station	slant distance (m)	α	S		
			screen	$1/R$[1]	Δ[2]
KIT	2251	0.85	1.8	3.4	-1.6
ARI	2359	0.81	4.6	7.7	-3.1
NAB	2657	0.96	1.4	1.8	-0.4
HAR	3401	0.57	4.4	11.7	-7.3
KUR	3572	0.97	(reference)		
JIG	3600	0.96	2.1	2.0	0.1
SET	4185	0.98	4.9	4.7	0.2
KOM	4546	0.96	1.3	1.4	-0.1
SVO	6218	0.60	0.3	3.3	-3.0

[1] $1/R$: geometrical spreading

[2] Δ: difference between the values of screen and $1/R$

Supplementary file

In Section 3, the relative amplitudes at the infrasound stations of Sakurajima volcano were calculated using the proposed theoretical method and compared with the observed values. Amplitudes of 0.5 Hz in the frequency domain were employed. The homogeneous speed of sound in air was assumed to be 340 m/s. These conditions are reflected in the wavenumber k $(= 2\pi/(c/f))$ shown in Eq. (5). Here, we investigated the effect of different 1) frequency and 2) sound speed values on the results of our method. In addition, 3) the effect of 3-D topography, which was not considered by the screen, was computed using a 3-D numerical simulation.

1) Frequency

An amplitude of 0.5 Hz in the frequency domain was used as the representative value in Section 3. However, the dominant frequency of observed data at some stations was 0.4 Hz (Fig. S1). Therefore, a frequency of 0.4 Hz was used to compute the synthetic amplitudes and compare them with the observed data in the same way as that shown in Fig. 3c.

2) Sound speed

The speed of sound in air was assumed to be 340 m/s in Section 3. However, the effective sound speed depends on the atmospheric temperature and wind speed. Therefore, we investigated how wide the range of estimated amplitudes can be made by varying the effective sound speed. The maximum/minimum temperatures and the maximum wind speed recorded in September 2017 at the JMA station, located 10 km west of the crater, were 34.6/17.7 ℃ and 22.8 m/s, respectively. Considering these temperatures, the effective sound speed in air was 342.1–351.9 m/s for a no-wind condition. Considering the wind data (i.e., headwind and tailwind at 22.8 m/s), the range of the effective sound speed can be further increased to 319.3–374.7 m/s. The end-members of the range of relative amplitudes can be estimated by using the maximum and minimum sound speeds toward the reference and target stations, respectively (and vice versa).

3) Effect of 3-D topography

A 3-D numerical simulation of infrasound propagation was performed to investigate the impact of 3-D topography, which was not included in the screen approximation. We used the infraFDTD code (Kim and Lees, 2014) for the calculation. The elevation model of Sakurajima was a 5-m DEM, equal to that for the screen approximation. The source time function was assumed to be a harmonic monopole source (peak frequency $f = 0.5$ and 0.4 Hz). The profile of the sound speed was a 1-D vertical structure, in which sound speed at the ground surface was 346.6 m/s based on the average temperature in September 2017 at the JMA station, and its gradient was assumed to be -0.05 (m/s)/m (National Oceanic and Atmospheric Administration et al., 1976). The calculation time step was 0.005 s and the duration was 40 s. For comparison with the observed values, the relative amplitudes in the frequency domain were transformed from the waveform of the 10-s window from 2 s before the arrival time of signals as well as the observed data.

The results of these investigations are summarized as follows and shown in Fig. S2. The standard deviation distances S are listed in Table S1.

1) The estimated relative amplitudes of 0.4 Hz (Fig. S2b) are closer to the observed distribution than those of $1/R$ (geometrical spreading), indicating the same result as the estimation at 0.5

Hz (Fig. 3c). Therefore, as long as the dominant frequency is used, it is confirmed that our method can more accurately estimate relative amplitude than the method that only considers geometrical spreading. However, we note that the relative amplitudes estimated using a screen less change between 0.5 and 0.4 Hz than the observed data (Fig. S2). Ignoring 3-D topography in the proposed method may be one of the causes of such a difference in the sensitivity to frequency changes. Therefore, a lot of care would be needed to apply this method when signals have no obvious dominant frequency common to all stations.

2) The variation of relative amplitude due to a change in effective sound speed (error bars in Fig. S2) is not significant. This result implies that the discrepancies between the observations and the estimates at ARI, HAR, and SET stations (Fig. 3c) are not due to the effective sound speed.

3) The relative amplitudes of the 3-D numerical simulation fall within the range of the observed distribution ($\pm 3\sigma$), suggesting that the discrepancies between observations and estimates at ARI, HAR, and SET stations (Fig. 3c) are mainly caused by ignoring the 3-D topography. Therefore, for a more precise estimation, it may be necessary to include some additional procedures in the proposed method. For example, the method should consider interaction between sound waves and asymmetric crater walls (Kim et al., 2012) or uneven ground surfaces.

Reference

Kim, K., Lees, J. M., 2014. Local volcano infrasound and source localization investigated by 3D simulation. Seismological Research Letters 85 (6), 1177–1186.

Kim, K., Lees, J. M., Ruiz, M., 2012. Acoustic multipole source model for volcanic explosions and inversion for source parameters. Geophysical Journal International 191 (3), 1192–1204.

National Oceanic and Atmospheric Administration, National Aeronautics and Space Administration, United States Air Force, 1976. US standard atmosphere, 1976. US Government Printing Office, Washington DC.

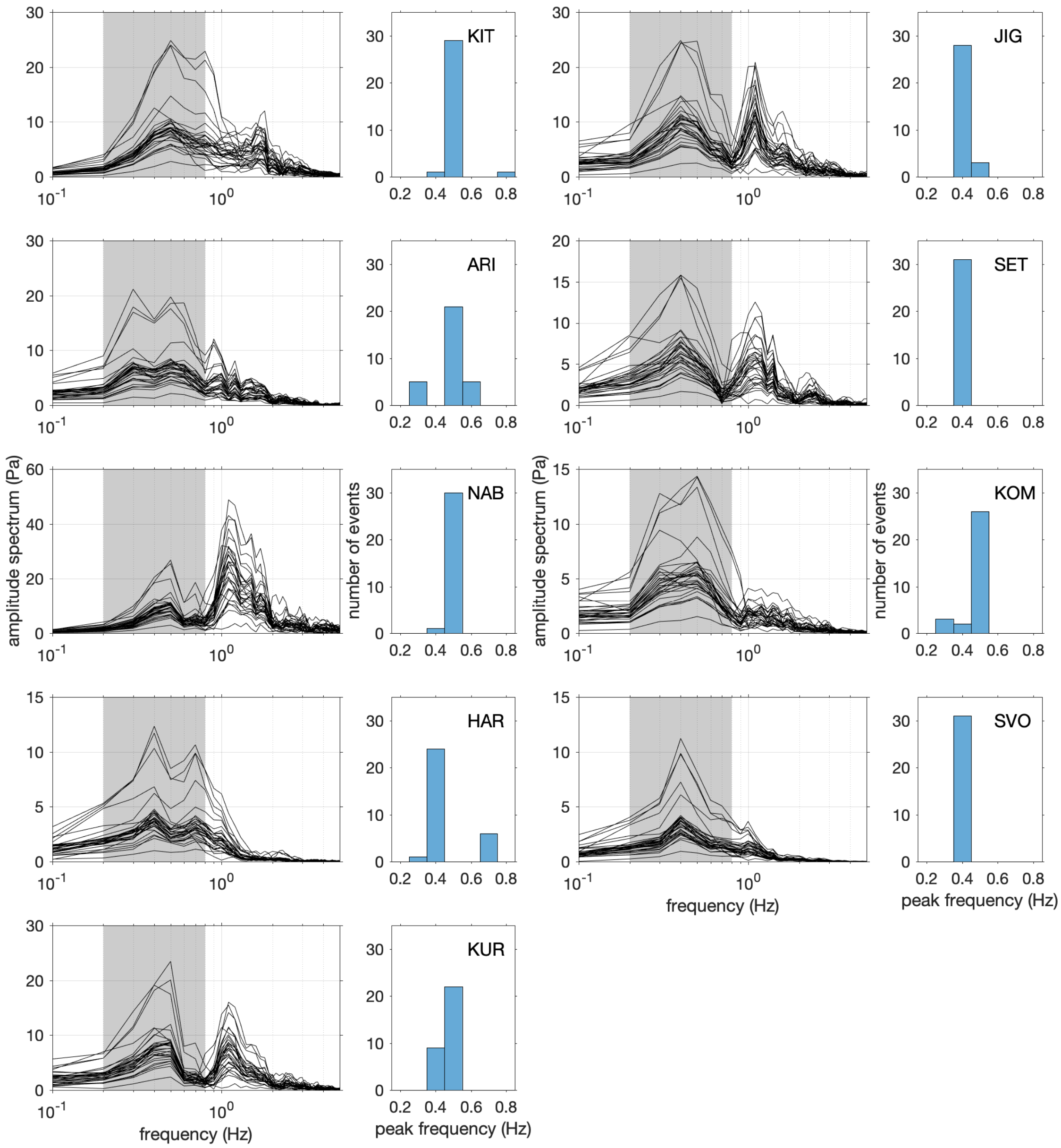

Figure S1: Amplitude spectra of infrasound signals observed around Sakurajima. Spectra are transformed from the 10-s waveform from 2 s before the arrival time. Histograms show the peak frequencies (in the range of 0.2–0.8 Hz; hatched area) of 31 events.

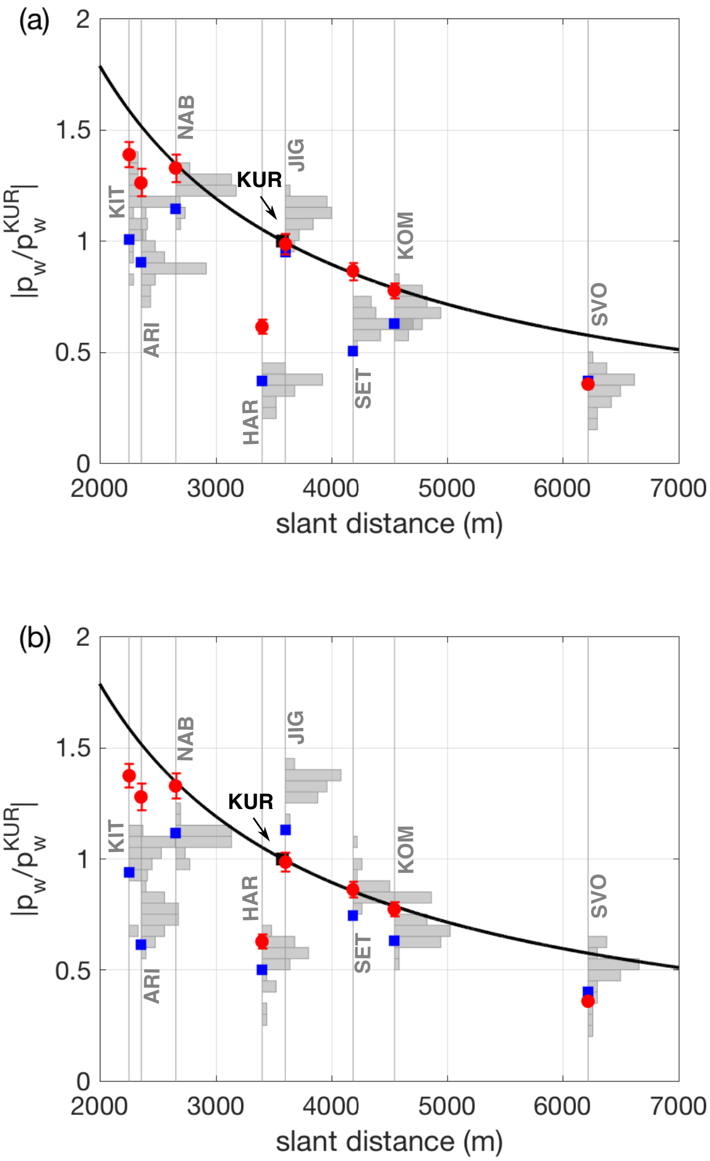

Figure S2: Comparison of relative amplitudes between estimates and observations. Red circles indicate our estimates using the screen approximation, and error bars show the ranges estimated using different effective sound speeds. Blue squares are the results of 3-D numerical simulation (FDTD). Black line represents the values derived by only considering geometrical spreading ($1/R$). (a) $f = 0.5$ Hz, and (b) $f = 0.4$ Hz.

Table S1: Standard deviation distances S at infrasound stations around Sakurajima volcano.

station	S ($f = 0.5$ Hz)			S ($f = 0.4$ Hz)		
	$1/R$	screen	FDTD	$1/R$	screen	FDTD
KIT	3.4	1.8	1.1	5.5	3.5	0.7
ARI	7.7	4.6	0.2	10.4	7.2	1.7
NAB	1.8	1.4	1.8	4.8	4.5	0.5
HAR	11.7	4.4	0.4	5.4	0.9	0.5
KUR			(reference)			
JIG	2.0	2.1	2.7	7.0	7.1	4.2
SET	4.7	4.9	2.8	0.0	0.1	2.0
KOM	1.4	1.3	1.0	2.5	2.2	0.6
SVO	3.3	0.3	0.5	0.9	1.3	1.9